# Mineralogical and geochemical evolution of a basalt-hosted fossil soil (Late Triassic, Ischigualasto Formation, northwest Argentina): Potential for paleoenvironmental reconstruction

**Neil J. Tabor**†
*Department of Geological Sciences, Southern Methodist University, Dallas, Texas 75275-0395, USA*

**Isabel P. Montañez**
**Robert Zierenberg**
*Department of Geology, University of California, Davis, California 95616, USA*

**Brian S. Currie**
*Department of Geology, Miami University, 114 Shideler Hall, Oxford, Ohio 45056, USA*

## ABSTRACT

**Reconstruction of paleoclimatic conditions in the Ischigualasto basin, northwestern Argentina, has been constrained by field studies coupled with mineralogic, whole-rock, and fine-fraction chemical and stable isotope analysis of a Triassic (Carnian) basalt-hosted fossil soil. Field evidence, such as wedge-shaped aggregate structure and slickensides, indicate this was likely a paleo-Vertisol. Whole-rock analysis defines down-profile trends in clay mineralogy and chemical composition that are consistent with modern soils developed upon basalt parent material. X-ray diffraction analysis indicates that the basaltic parent material is dominated by plagioclase with trace amounts of weathered 2:1 phyllosilicate. Overlying weathered horizons show a progressive loss of plagioclase and an increase in phyllosilicates with minor amounts of kandite clays and detrital quartz. X-ray diffraction analysis of the <2 μm fraction shows that the weathered layers are dominated by dioctahedral smectite (montmorillonite) with a minor fraction of kaolinite in the upper layers of the profile. There is a progressive loss of basic cations in conjunction with an increase in concentration, on a wt% basis, of conservative elements from the basalt upward through the weathering profile. The combined data indicate that this soil likely formed on a stable landscape in a cool and humid climate. In addition, the presence of quartz in the paleosol profile suggests an eolian contribution of sediment during pedogenesis.**

**Despite these apparent morphologic and bulk chemical trends indicative of a pedogenic origin, none of the authigenic minerals formed in isotopic equilibrium. However, based on measured oxygen and hydrogen isotope compositions, these minerals apparently formed from meteoric waters with a narrow range of $\delta^{18}O$ and $\delta D$ compositions at different temperatures. If this is correct, then amygdaloidal calcites formed at ~60–100 °C, followed by precipitation of montmorillonites at 49–57 °C during late-stage hydrothermal alteration. Finally, goethite formed at low temperatures of 6 ± 3 °C in a pedogenic environment.**

**This complex history of hydrothermal alteration and pedogenic overprinting brings to light the need for cautious interpretation of bulk chemical trends in paleosols as a means for paleoclimate reconstruction. Comparison of the calculated Triassic oxygen isotopic compositions of meteoric water and soil temperature with modern environments suggests that this soil formed in a seasonal, humid, and cool climate.**

**Keywords: paleosols, clay mineralogy, oxygen and hydrogen isotopes of pedogenic minerals, paleoclimate, mineral weathering.**

## INTRODUCTION

In a detailed isotopic study of modern weathering and soil profiles developed on igneous parent rock, Lawrence and Taylor (1971, 1972) found that the D/H and $^{18}O/^{16}O$ ratio of a given authigenic clay mineral or hydroxide remains constant throughout the entire soil profile, indicating that the minerals formed at or near isotopic equilibrium with soil waters. Furthermore, Savin and Epstein (1970) and Lawrence and Taylor (1971, 1972) established that the isotopic composition of authigenic phyllosilicates and hydroxides from modern soil profiles exhibit $\delta D$ and $\delta^{18}O$ values that parallel the modern meteoric waterline. This supports a meteoric origin for waters involved in subaerial weathering environments and indicates that the isotopic composition of soil-formed minerals that develop on igneous parent rock are generally not compromised by inherited clay minerals or hydroxides. Therefore, the isotopic composition of hydrated minerals that form in igneous rock–hosted soils may provide environmental information for the time of weathering, and the relationship between the isotopic composition of soil-formed minerals in igneous-hosted fossil soils and the paleometeoric waterline hold potential for quantifying paleoclimatic conditions.

Extrusive igneous deposits are an important lithologic component of many depositional basins (e.g., Newark Basin, Siberian and Deccan Traps, East African Rift). Pedogenic minerals formed on igneous lithologies in sedimentary basins, if critically assessed, have the potential to yield significant paleoclimate information. To date, however, no chemical and isotopic analysis of ancient soil-formed minerals developed upon igneous materials has been presented. Here, we provide the first detailed mineral, chemical, and stable isotope ($\delta D$ and $\delta^{18}O$) study of a Triassic soil profile developed on a basalt flow from the Ischigualasto–Villa Unión basin of northwest Argentina (Fig. 1).

The results indicate that many of the original macro- and micromorphological weathering features remain intact in the Triassic-age paleosol.

†E-mail: ntabor@mail.smu.edu.

*GSA Bulletin*; September/October 2004; v. 116; no. 9/10; p. 1280–1293; doi: 10.1130/B25222.1; 10 figures; 4 tables; Data Repository item 2004128.

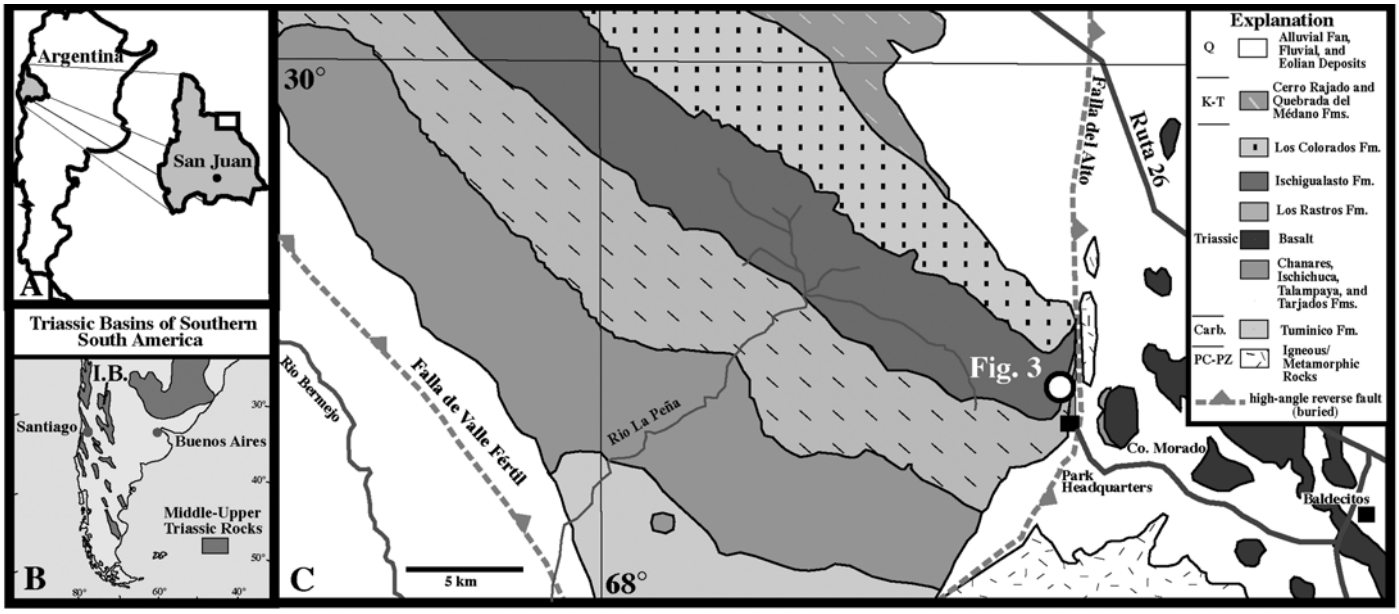


**Figure 1. Location maps of the Ischigualasto basin. (A) Map of San Juan Province, Argentina. White rectangle shows location of Figure 1C. (B) Distribution of Triassic basins in southern South America. "I.B." marks the position of the Ischigualasto–Villa Unión basin in northwest Argentina. (C) Geologic map of the southern part of the Ischigualasto–Villa Unión basin. White circle shows location of measured section in Figure 3.**

Furthermore, geochemical trends in the weathering profile are consistent with commonly observed pedogenic weathering environments (e.g., Tardy, 1971). The suite of authigenic minerals preserved in the weathering profile are not in isotopic equilibrium, contrary to what was expected based on investigations of modern soil-weathering environments. However, the isotopic data do indicate that this suite of minerals formed from the same meteoric waters during hydrothermal alteration and subsequent low-temperature pedogenic overprinting. Although the paragenetic sequence of mineral formation in basalt flows may be quite complex, this study shows that climate reconstructions may still be made from these geologically abundant lithologies.

## GEOLOGIC BACKGROUND

### Tectonic Setting and Stratigraphy

The study area is located along the southern edge of the Ischigualasto–Villa Unión basin in northeastern San Juan Province, Argentina, and lies within the boundaries of the Ischigualasto Provincial Park (Fig. 1). During Mesozoic time, oceanic-continental plate interactions along the southwestern margin of Pangea produced a region of extensional deformation cratonward of the proto-Andean magmatic arc (Ramos and Kay, 1991; Lopez-Gamundi et al., 1994). Extension was focused along the northwest-trending boundary between Paleozoic accreted terranes and the Precambrian Gondwanan craton (Uliana et al., 1989). The Ischigualasto–Villa Unión basin of northwest Argentina is one of a series of continental-rift basins that developed in the region as a result of this extension (Fig. 1B) (Uliana and Biddle, 1988).

The rocks of the Ischigualasto–Villa Unión basin are exposed adjacent to the Valle Fertíl and Alto faults, both of which are interpreted to be Triassic normal faults that were reactivated in the Neogene with reverse displacement (Fig. 1C) (Milana and Alcober, 1994). Rift-related deposition in the Ischigualasto–Villa Unión basin began during Early Triassic time. Rifting continued into the Cretaceous, providing accommodation space for accumulation of >4 km of nonmarine and volcanic strata (Milana and Alcober, 1994; Alcober, 1996). The Triassic system in the basin consists of the Lower Triassic Talampaya and Tarjados Formations, the Middle Triassic Chañares/Ischichuca and Los Rastros Formations, and the Upper Triassic Ischigualasto and Los Colorados Formations (Fig. 2) (Stipanicic and Bonaparte, 1979). The paleosol that is the focus of this investigation is stratigraphically situated near the base of the Ischigualasto Formation (Fig. 3) (Currie et al., 2001).

In the study area, the Ischigualasto Formation consists of ~300–700 m of mudstone, sandstone, conglomerate, and basalt. The sedimentary rocks of the formation are primarily channel and overbank deposits of fluvial systems sourced in Triassic highlands southwest of the Valle Fertíl paleofault, whereas the basalts were formed by flows originating from volcanic centers located at the northeast and northwest margins of the basin (Alcober, 1996).

An Upper Triassic age of the Ischigualasto Formation is based on vertebrate fossils and a radiometric age of altered ash beds from the unit. Abundant vertebrate fossils from the lower two-thirds of the formation indicate a Carnian age of deposition (Rodgers et al., 1993; Alcober, 1996), whereas $^{40}Ar/^{39}Ar$ dating of sanidine crystals from a bentonite ~80 m above the base of the formation yielded an age of 227.8 ± 0.3 Ma (Rodgers et al., 1993). In addition, to the east of the study area near Baldecitos (Fig. 1C), basalt flows correlated with the Landinian Los Rastros Formation yielded a K/Ar age of 229 ± 5 Ma (Fig. 2) (Valencio et al., 1975; Odin et al., 1982). Collectively, these ages support a Carnian age of deposition for the lower part of the Ischigualasto Formation (Fig. 2).

The thickness of overlying units north of the study area indicates that <2 km of additional Jurassic-Tertiary strata were deposited in the basin following Triassic deposition (Stipanicic and Boneparte, 1979). This interpretation is supported by geochemical analysis of organic-rich shales from the Los Rastros Formation in the southern part of the basin that indicate that burial depths of the Middle Triassic stratigraphic interval did not exceed 2 km (Lopez, 1995). The rocks of the basin are presently exposed as a result of Miocene-Holocene reverse-displacement reactivation of

the Valle Fertíl and Alto faults (Milana and Alcober, 1994).

### Paleoclimatic Interpretation of the Ischigualasto Basin Sedimentary Sequence

During the Triassic, the Ischigualasto basin was situated at mid-latitudes (40°–50° S), along the southwestern edge of Gondwana (Scotese and Golonka, 1992; Smith et al., 1994). Previous workers identified a single climate cycle, from relatively dry and seasonal during the Early Triassic, to more humid during Middle Triassic deposition, then returning to seasonally dry during the Late Triassic (Stipanicic and Bonaparte, 1979; Alcober, 1996). These interpretations are based primarily on sedimentological and paleontological evidence such as the presence of red beds and braided ephemeral stream and eolian deposits in the Lower Triassic Tarjados/Talampaya Formations (Lopez-Gamunidi et al., 1989), abundant lacustrine deposits and preserved plant fossils in the Middle Triassic Chañares/Ischichuca and Los Rastros Formations, and red beds, calcareous paleosols, and evaporite deposits in the Upper Triassic Ischigualasto and Los Colorados Formations (Stipanicic and Bonaparte, 1979; Alcober, 1996). In these interpretations, the lowermost lacustrine strata of the Ischichuca Formation represent the wettest Triassic interval, while the uppermost Los Colorados Formation represents the driest interval (Alcober, 1996). The Ischigualasto Formation, therefore, represents deposition during the transition between these interpreted "wettest" and "driest" intervals.

## METHODS

The paleosol that is the focus of this investigation is stratigraphically situated ~45 m above the base of the Ischigualasto Formation in the eastern part of the Ischigualasto Provincial Park (Figs. 1C, 3, and 4). The paleosol profile was logged and described in the field according to the methods of Retallack (1988). This unit is composed of loosely consolidated mudstones and claystones above an ~8.5-m-thick basalt flow. In order to avoid recent weathering products not associated with Triassic weathering, the outcrop face was excavated ~60 cm to provide a fresh surface for describing and sampling. Approximately 500 g of material were collected from each unit within the paleosol and stored in canvas bags. In addition, indurated Fe oxides were collected from narrow (~2 cm) ironstone bands occluding joint fractures within the basalt ~1.0 to 1.5 m beneath the surface of the paleosol. Detailed procedures and methods of mineralogical, chemical, and isotope characterization

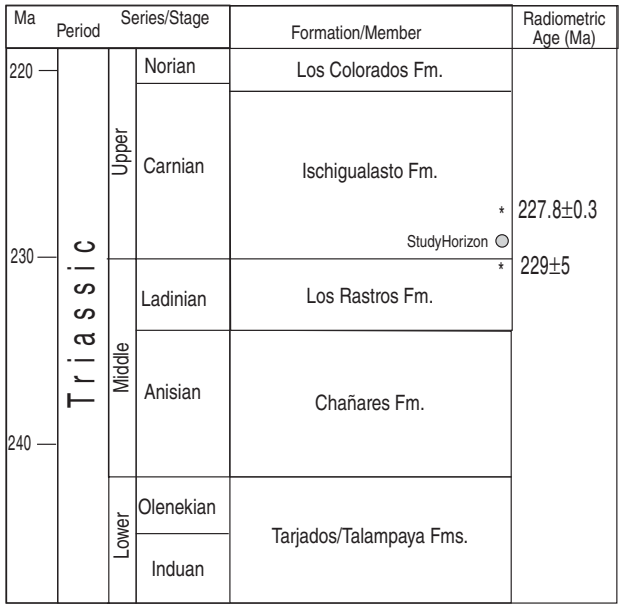


**Figure 2. Time-stratigraphic chart for Triassic rocks of the Ischigualasto–Villa Unión basin and relative stratigraphic position of studied paleosol and radiometrically dated horizons. Time scale adapted from Alcober (1996).**

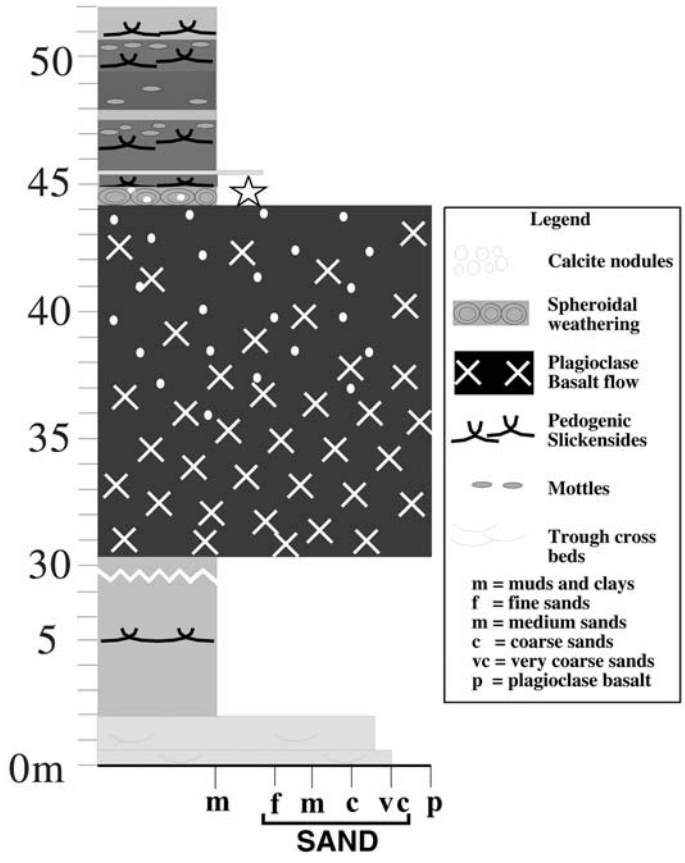


**Figure 3. Measured section of the basal Ischigualasto Formation from the eastern region of Ischigualasto Provincial Park. Meter level corresponds to height above the base of the formation. The studied paleosol occurs at ~44–45 m (star) in the upper part of a thick basalt. See legend for explanation of lithologic symbols.**

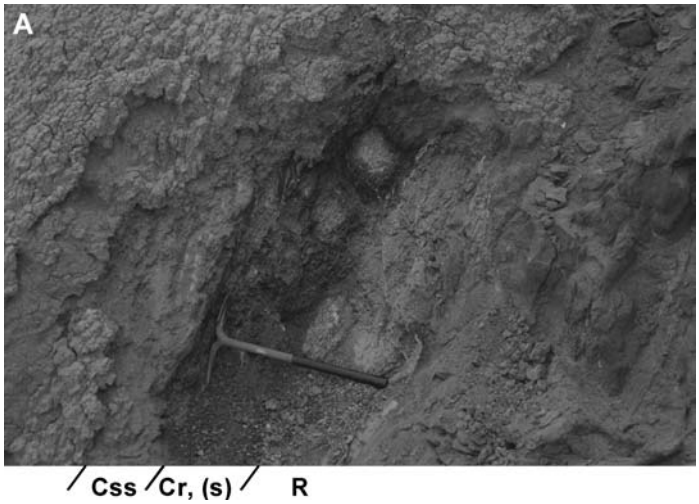


**Figure 4. (A) Field photograph of the Carnian-age basalt flow and overlying weathered horizon (structural dip of ~50°). The spheroidal zone is recognized in the layer above the basalt by the gray spheroidal centers in the middle of the photograph. Pick for scale (75 cm). The horizon designations R, Cr, and Css correspond to the nomenclature of the Soil Survey Staff (1998). The descriptors (S) and (s) refer to the spheroidal weathering zone. (*Figure 4 continued on following page.*)**

and analysis of the samples are available but are not discussed further in this manuscript.[1]

## RESULTS

### Paleosol Morphology

A clay-rich deposit defines the upper 53 cm of an ~14-m-thick basalt flow (Fig. 3). The lower 8 m is massive, unweathered, vesicular, holocrystalline plagioclase basalt (R in Fig. 4). Some vesicles are open and others have been filled by calcite amygdules. The upper 1.0 to 1.5 m of the basalt flow exhibits areas of extensive jointing and fractures that are commonly filled with reddish-brown to black Fe oxide minerals. A 23- to 32-cm-thick zone of spheroidal concentric alteration (Cr in Fig. 4) overlies the unweathered basalt (R). The outer "rinds" of the spheroids are clay-rich and friable, 4 to 8 cm thick, and consist of dusky red, clay-altered basalt with massive to weakly developed fine angular blocky structure (D in Figs. 4B–C). The middle rinds are 5 to 6 cm thick, greenish gray, and friable with poorly preserved calcite amygdules and waxy, green, phyllosilicate amygdules. The cores of the spheroid are light gray and range from 8 cm to 11 cm in diameter (C in Figs. 4B–C). The interiors of the spheroids are less friable and preserve calcite amygdules. There is a distinct (2–5 cm thick) transition from the spheroidal zone to a 20–30 cm thick, massive, dusky red noncalcareous layer with wedge-shaped aggregate structure and slickensides (E; Css horizon in Fig. 4). This upper layer has an abrupt and wavy upper boundary overlain by thin, cross-bedded fine sandstone.

### Mineralogy

The unweathered basalt consists primarily of acicular plagioclase crystals ranging from 0.5 to 1 mm long and 75 to 200 μm wide in a fine-grained groundmass of pyroxene, plagioclase, and iron-titanium oxide (Fig. 5A). Plagioclase crystals show a high degree of orientation defining a flow banding that is parallel to over- and underlying sedimentary bedding. The basalt also contains 3 to 5 vol% (by point count) ilmenite crystals (Fig. 5A).

Basalt directly underlying the spheroidal weathering zone contains a significant amount of secondary calcite, phyllosilicate, and Fe oxide minerals (Figs. 5B–D). Isopachous calcite spar with dull luminescence lines to completely fills primary vesicles and secondary porosity within the basalt (Figs. 5B–C). In some instances, calcite fills voids formed by dissolution of plagioclase crystals (Fig. 5C). Pores incompletely filled by calcite contain botryoidal phyllosilicate precipitates (Fig. 5B), indicating that calcite precipitated first in the vesicles. Reflected light microscopy shows alteration of pyroxene and ilmenite to goethite (α-FeOOH; Fig. 5D). Phyllosilicate and iron oxide alteration products are observed along the perimeter of plagioclase laths (Fig. 5C). Phyllosilicates within calcite-filled vugs are Mg- and Fe-rich, whereas vug-filling calcite contains trace amounts of Mg and Fe. In addition, botryoidal goethite partially to entirely fills dissolution cavities developed in calcite amygdules, indicating that goethite formed subsequent to calcite under conditions that favored calcite dissolution.

X-ray diffractograms of the unweathered basalt (A in Fig. 6) reveal a sharp and intense peak at 3.21 Å, corresponding to the d(001) of plagioclase. In addition, a very broad peak near 13.7 Å indicates trace 2:1 phyllosilicates. Plagioclase peaks in the whole-rock fractions of the spheroidal weathering zone (B, C, and D in Fig. 6) show a progressive loss of intensity from the inner core-stones (B) of the spheroidally weathered zones outward through the inner (C) and outer (D) weathering rinds and upward into the overlying Css horizon (E in Fig. 6). All of these samples show relatively sharp and intense phyllosilicate d(001) peaks at ~12.65 Å. Furthermore, the outer rind of the Cr horizon (D in Fig. 6), and the Css horizon (E), exhibit minor peaks near 7.18 Å, likely indicating the presence of kandite clay (Moore and Reynolds, 1997). Both the outer weathering rind (D) and overlying Css horizon (E) exhibit low and sharp peaks at 3.33 Å and 4.26 Å, indicating the presence of quartz.

X-ray diffraction analysis of the <2 μm fraction from the unweathered basalt layer (A) displays a series of peaks (Fig. 7A). Magnesium-saturated samples exhibit intense and broad peaks at ~14 Å and 7.1 Å, whereas magnesium-saturated and glycerol-solvated samples exhibit two peaks at about 14 Å and 18 Å, with a broad plateau connecting the two peaks. Air-dried (25 °C) potassium-saturated samples exhibit broad peaks at about 14 Å and 7.1 Å, whereas the 500 °C potassium-saturated samples exhibit only low and broad peaks from 15 Å to 10 Å. In addition, there are sharp, but weak, peaks in all of the diffractograms at about 30 Å to 34 Å. This collective behavior is characteristic of interlayered chlorite/smectite, or corrensite (Moore and Reynolds, 1997).

The <2 μm fraction from the weathered zones (B–E) displays sharp and intense peaks (Figs. 7B–C). They all exhibit similar behavior with chemical and thermal treatments. The samples exhibit a 12.12–12.34 Å peak with $K^+$ saturation that shifts to 9.86–10.07 Å upon heating to 500 °C. These samples also exhibit sharp and intense peaks at 14.45–14.89 Å when $Mg^{2+}$-saturated that shift to 17.50–17.86 Å when glycerol solvated. This behavior corresponds to the presence of smectite. The d(060) analysis of these samples shows broad and low peaks

[1]GSA Data Repository item 2004128, supplemental methods, is available on the Web at http://www.geosociety.org/pubs/ft2004.htm. Requests may also be sent to editing@geosociety.org.

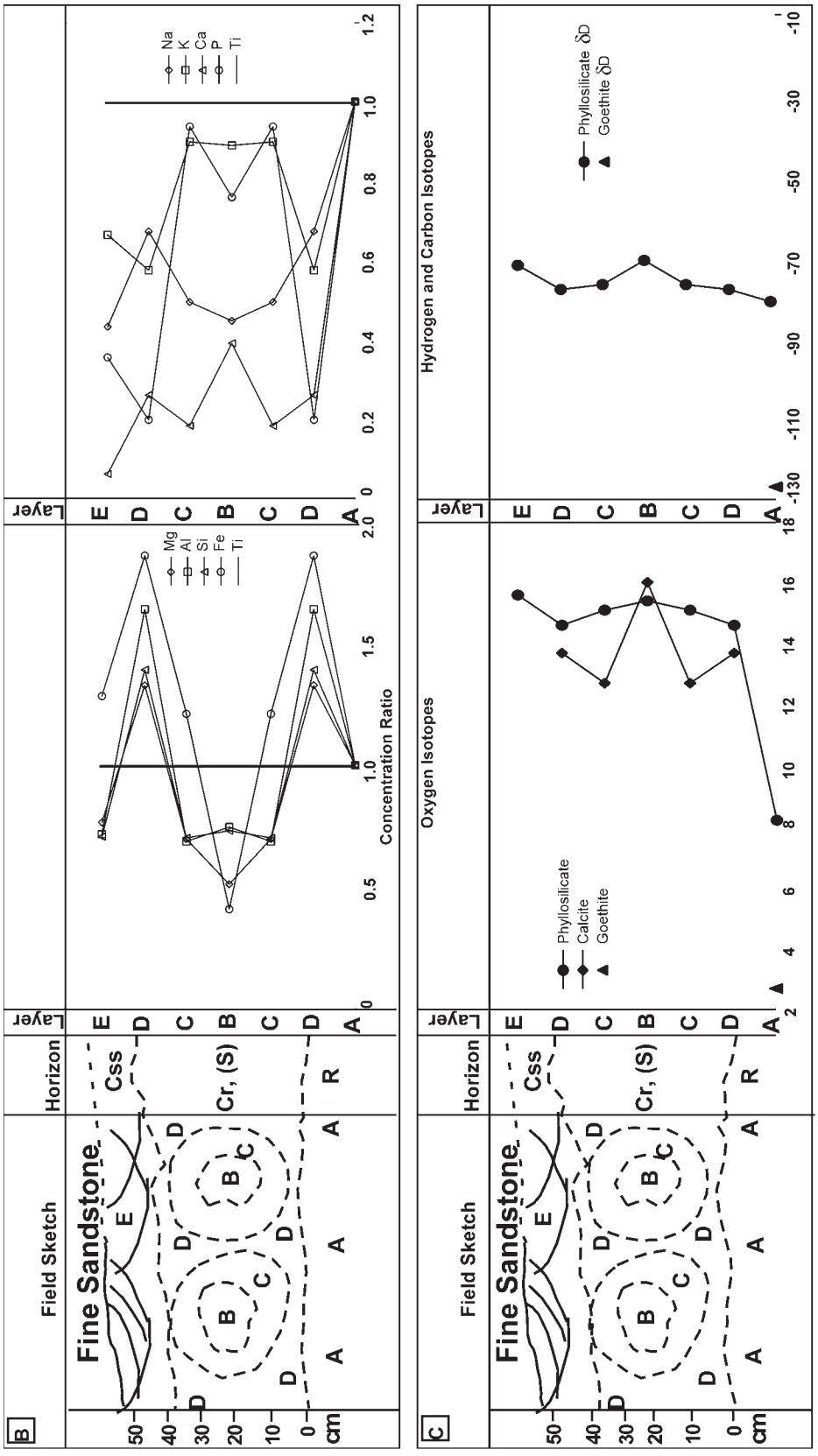


**Figure 4 (*continued*). (B) Schematic diagram of the weathered horizon and underlying basalt juxtaposed with the concentration ratios of oxides. See text for explanation. (C) Schematic diagram of the weathered horizon and underlying basalt juxtaposed with the oxygen and hydrogen isotope compositions of phyllosilicates, goethite, and calcite. See text for explanation. Letters A–E refer to the locations of samples analyzed by X-ray diffraction referred to in Figure 6 and throughout the text.**

near 1.50 Å (Fig. 7D), indicating they are dioctahedral montmorillonite (Brindley, 1980). Minor peaks at 7.14 and 7.18 Å in the <2 µm fraction of the outer spheroidal zone (D) and the Css horizon (E), respectively, do not shift with glycerol solvation and disappear with heating to 500 °C, indicating the presence of kaolinite (e.g., Fig. 7C and Moore and Reynolds, 1997).

X-ray diffraction of the bulk Fe oxide sample (Fig. 8) shows sharp and intense peaks corresponding to the crystallographic d(hkl) spacings of goethite (α-FeOOH). Within analytical uncertainty, (110) and (111) goethite d-spacings indicate 0% $Al^{3+}$ substitution in this sample (Schulze, 1984). Broad and poorly resolved peaks near 10.2 Å and 7.2 Å indicate trace 2:1 and 1:1 phyllosilicate minerals, respectively.

## Chemical Composition

Both the whole-rock and <2 µm chemical analyses show chemical trends consistent with chemical weathering in modern soil-forming systems. Whole-rock compositions of the basalt and the basalt-weathering zone are presented in Table 1. Chemical weathering in soils preferentially removes more labile elements (e.g., alkalis) and concentrates less soluble elements such as aluminum and titanium (Monro et al., 1983). Thus, higher concentrations of more immobile elements are found toward the soil surface where chemical weathering is most intense. Variations in the major elements in the weathering profile are normalized to the immobile conservative element titanium (cf. Retallack, 1990) and presented as concentration ratios defined as:

$$\text{concentration ratio of element} = \text{wt\% oxide}_{(x)} / \text{wt\% oxide}_{(ref)} * \text{wt\% Ti}_{(ref)} / \text{wt\% Ti}_{(x)},$$

where "x" denotes values within a given layer (e.g., layer E) and "ref" denotes values in the reference parent material (i.e., basalt in layer A).

In general, sodium, potassium, calcium, and phosphorus are less concentrated in the

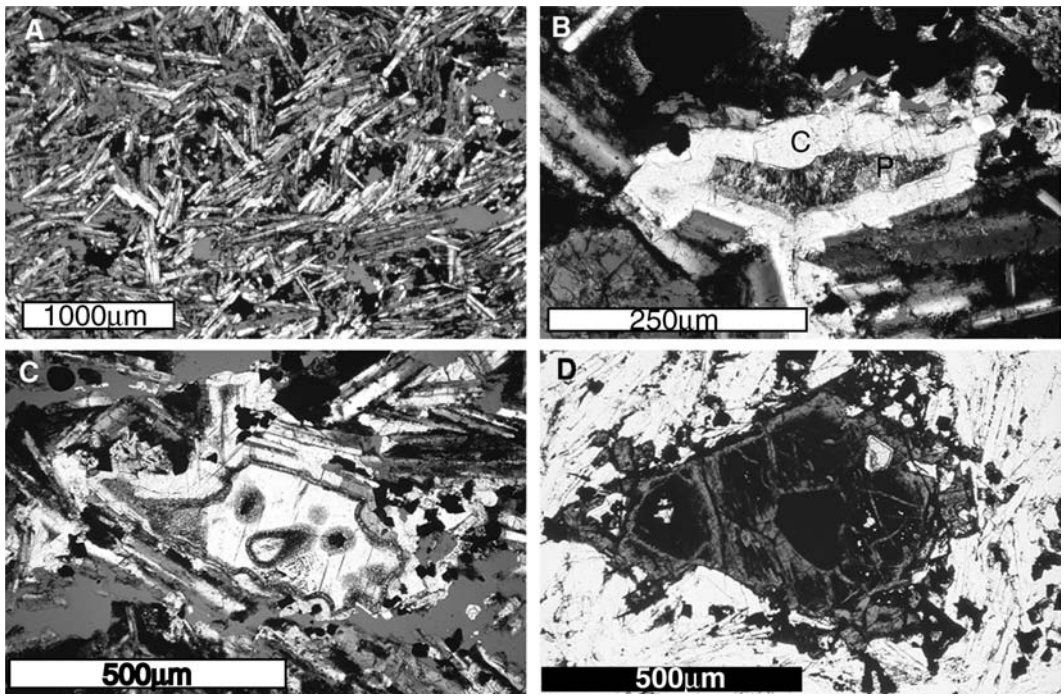


**Figure 5. Photomicrographs. (A) Plagioclase and ilmenite (opaques) crystals in host basalt. Plagioclase crystal laths show a high degree of orientation. (B) Isopachous drusy calcite (white) and phyllosilicate (center) void-fill in parent basalt. Plagioclase laths show weathering pits along perimeter of crystals. (C) Isopachous drusy calcite and calcite spar filling a vug in plagioclase basalt matrix. Some plagioclase crystals have phyllosilicate alteration rinds. (D) Ilmenite crystals (black) in plagioclase basalt (white) weathering to a latticework of fine-grained goethite (gray).**

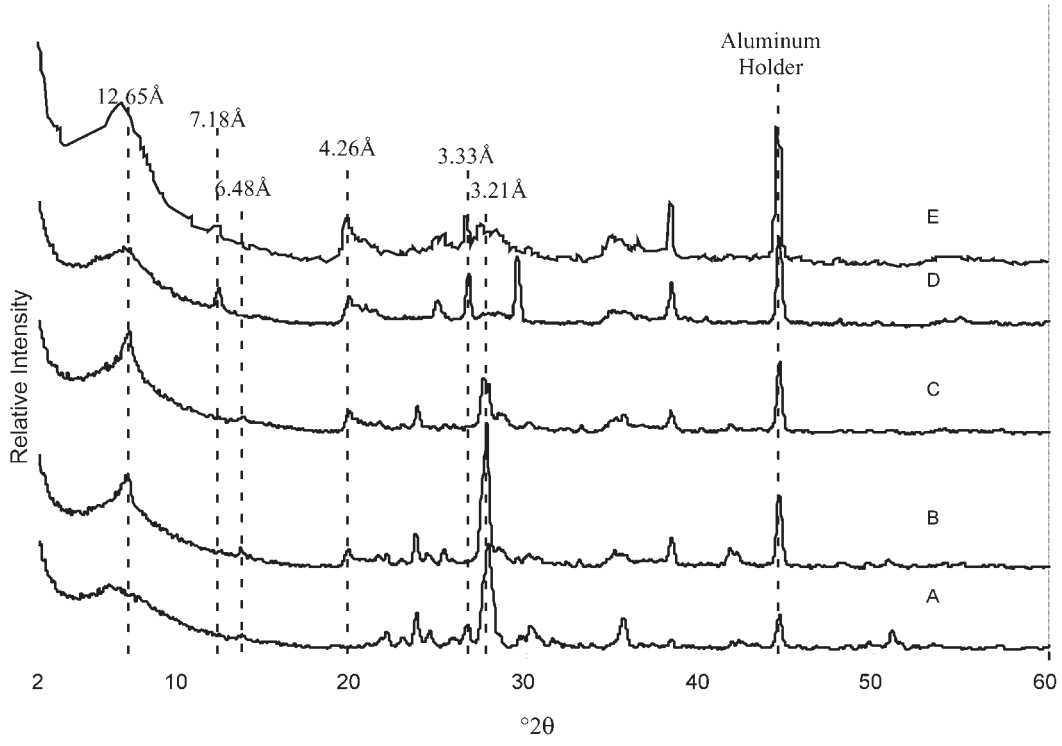


**Figure 6. X-ray diffractograms of the bulk fractions of the unweathered basalt (A), the spheroidal weathering zone (B–D) and the overlying Css horizon (E). The diffractograms are placed, from bottom to top, in order of increased weathering of the parent basalt. There is a progressive loss of plagioclase (3.21 Å and 6.48 Å) in conjunction with a gain in phyllosilicates (12.65 Å). (D) and (E) show a low and broad peak at ~7.18 Å, indicating kandite clays, and peaks at 4.27 Å and 3.33 Å that indicate quartz.**

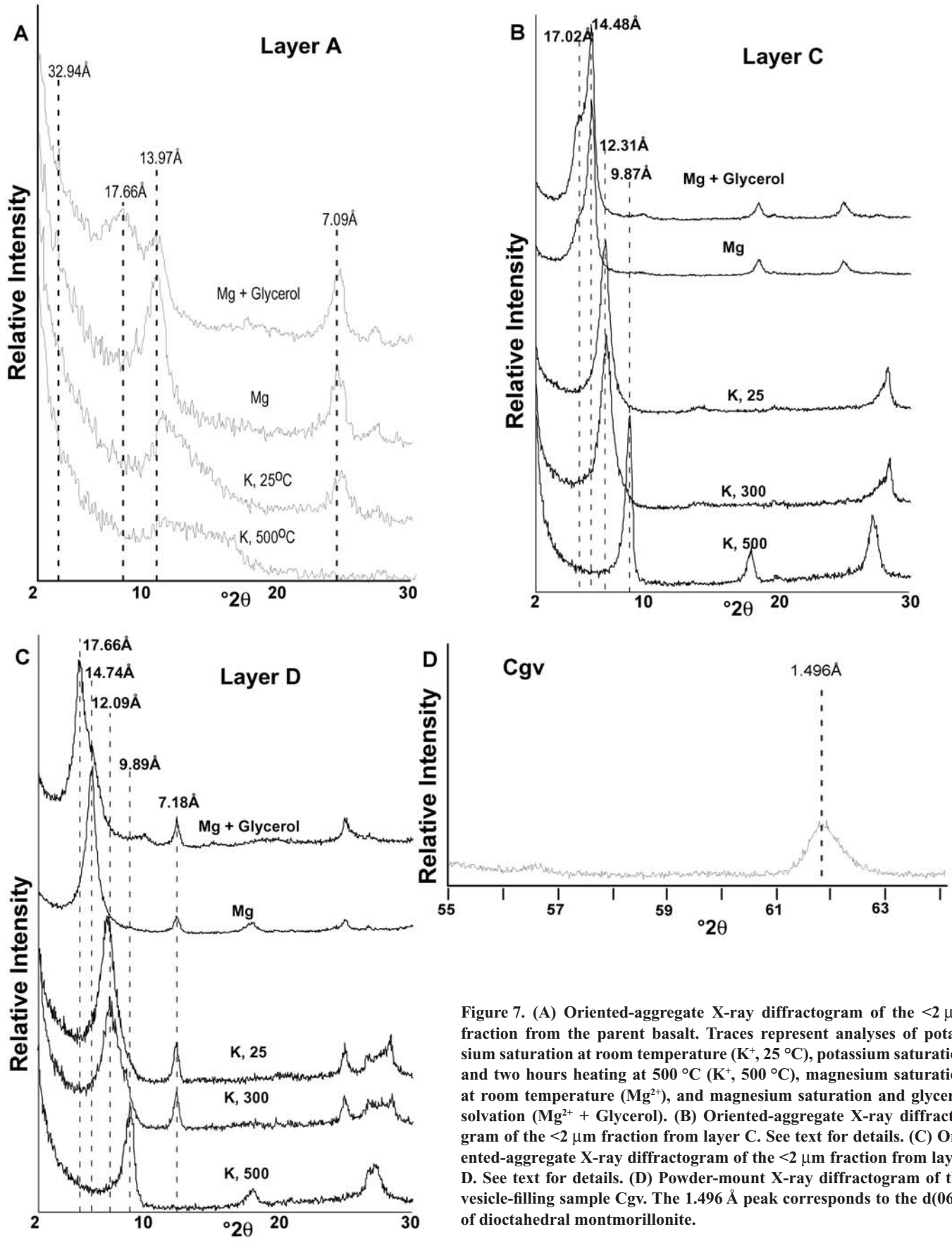


**Figure 7. (A) Oriented-aggregate X-ray diffractogram of the <2 μm fraction from the parent basalt. Traces represent analyses of potassium saturation at room temperature ($K^+$, 25 °C), potassium saturation and two hours heating at 500 °C ($K^+$, 500 °C), magnesium saturation at room temperature ($Mg^{2+}$), and magnesium saturation and glycerol solvation ($Mg^{2+}$ + Glycerol). (B) Oriented-aggregate X-ray diffractogram of the <2 μm fraction from layer C. See text for details. (C) Oriented-aggregate X-ray diffractogram of the <2 μm fraction from layer D. See text for details. (D) Powder-mount X-ray diffractogram of the vesicle-filling sample Cgv. The 1.496 Å peak corresponds to the d(060) of dioctahedral montmorillonite.**

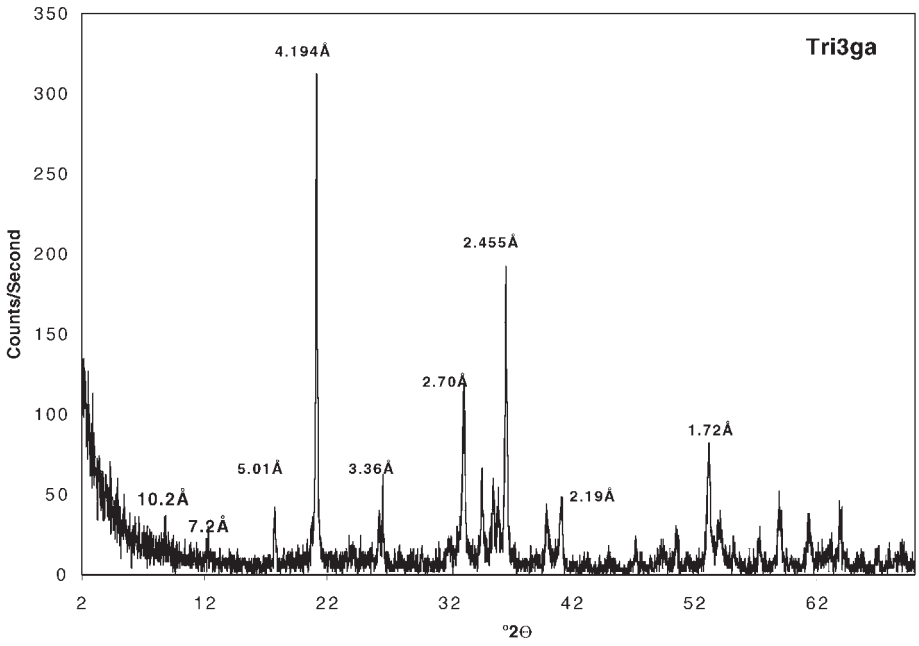


**Figure 8. Powder-mount X-ray diffractogram of goethite taken from weathering profile. The Å values for the (110) and (111) peaks are reported with three decimal places from a high-resolution, long-duration X-ray analysis. The 2:1 and 1:1 phyllosilicate peaks are reported with only one decimal place due to the low and broad (00l) peaks for this analysis. The combination of peaks indicates that the sample is dominated by goethite with trace amounts of 2:1 phyllosilicate.**

TABLE 1. ELEMENTAL COMPOSITION OF FUSED GLASSES AND WT% $H_2O$ OF SAMPLES IN THIS STUDY

| Sample | Size fraction | $Na_2O$ | MgO | $Al_2O_3$ | $SiO_2$ | $P_2O_5$ | $K_2O$ | CaO | $TiO_2$ | $Fe_2O_3$ | Total | wt% $H_2O$ |
|---|---|---|---|---|---|---|---|---|---|---|---|---|
| A | Bulk | 4.41 | 2.48 | 19.54 | 52.85 | 0.40 | 1.67 | 7.74 | 3.45 | 6.52 | 99.06 | 1.18 |
| B | Bulk | 2.29 | 1.91 | 21.54 | 56.79 | 0.50 | 2.24 | 3.93 | 5.14 | 3.94 | 98.28 | 2.81 |
| C | Bulk | 2.35 | 2.41 | 21.77 | 51.88 | 0.52 | 2.09 | 1.71 | 4.82 | 11.03 | 98.58 | 3.23 |
| Cgv | Bulk | 2.25 | 3.97 | 22.51 | 61.68 | B.D. | 0.33 | 0.25 | 0.45 | 6.56 | 98.00 | 4.22 |
| D | Bulk | 1.74 | 2.51 | 24.50 | 56.15 | 0.02 | 0.73 | 1.32 | 2.62 | 9.26 | 98.85 | 5.41 |
| E | Bulk | 2.08 | 2.68 | 21.78 | 52.64 | 0.20 | 1.57 | 0.56 | 4.88 | 11.89 | 98.28 | 4.30 |
| B | <2 μm | 1.88 | 3.48 | 22.90 | 60.08 | B.D. | 0.97 | 0.71 | 2.55 | 5.78 | 98.35 | 4.39 |
| C | <2 μm | 2.06 | 3.36 | 22.54 | 59.31 | B.D. | 1.51 | 0.79 | 1.86 | 6.60 | 98.03 | 4.75 |
| D | <2 μm | 1.72 | 2.97 | 23.41 | 61.82 | B.D. | 1.51 | 0.12 | 1.11 | 7.13 | 99.79 | 5.23 |
| E | <2 μm | 1.58 | 3.07 | 22.88 | 57.91 | B.D. | 1.68 | 0.31 | 3.53 | 7.37 | 98.33 | 4.65 |
| St. dev.* | | 0.08 | 0.06 | 0.08 | 0.32 | 0.04 | 0.05 | 0.05 | 0.01 | 0.23 | | |

*Note*: B <2 μm fraction: $(Ca_{0.01}Na_{0.20}K_{0.10})(Al_{1.40}Mg_{0.27}Fe_{0.33}Ti_{0.05})(Si_{3.73}Al_{0.27})$. C <2 μm fraction: $(Ca_{0.01}Na_{0.25}K_{0.12})(Al_{1.34}Mg_{0.31}Fe_{0.31}Ti_{0.09})(Si_{3.69}Al_{0.31})$. Cgv: $(Ca_{0.02}Na_{0.26}K_{0.02})(Al_{1.33}Mg_{0.35}Fe_{0.30}Ti_{0.02})(Si_{3.78}Al_{0.22})$. B.D.—concentrations below detection limits.

*Standard deviations (1σ) around the mean (n = 6).

weathered layers B through E relative to the underlying unaltered parent basalt (Fig. 4B). Observed concentration ratios, however, define complex trends. Concentration ratios for K and Ca are highest in the core-stone of the spheroid despite a more proximal position to the weathering surface than portions of layers C and D. Concentration ratios of Mg, Al, Si, and Fe are enriched in layer D, whereas only Fe is enriched in layers C and E and the inner core-stone (B) is depleted in all element ratios relative to the basalt parent material (Fig. 4B).

The whole-rock fraction exhibits up-profile trends in mineral-bound water that reflect greater concentrations of secondary alteration products. There is a progressive increase in wt% $H_2O$ from the unweathered basalt (A: 1.18 wt%) through the spheroidal weathering zone (B: 2.81 wt%) (C: 3.23 wt%) (D: 5.41 wt%), up through the overlying Css horizon (E: 4.30 wt%; Table 1). The low wt% $H_2O$ in the basalt sample (A) reflects the relatively low phyllosilicate concentration (Fig. 7). The high wt% $H_2O$ from the outer rind (D) of the spheroidally weathered zone (Cr horizon), in conjunction with high Al contents in the <2 μm fraction (Table 1), suggests a minor concentration of oxyhydroxide (e.g., gibbsite), unrecognized by X-ray diffraction.

Microprobe analysis of the <2 μm alteration products within the parent basalt indicates at least two different phyllosilicates—a magnesium-poor and a magnesium-rich phyllosilicate mineral (Fig. 5B; Table 2). The magnesium-poor phyllosilicate is associated with direct alteration of plagioclase feldspar crystals (Figs. 4A–C), whereas the magnesium-rich phyllosilicate occurs with other vesicle-filling minerals. High wt% $Fe_2O_3$ and $TiO_2$ in the magnesium-poor samples suggest they probably also contain admixed oxide phases. The Mg-rich phyllosilicates are likely chlorite/smectite, or corrensite, whereas the Mg-poor phyllosilicates are probably montmorillonitic smectites. However, we were not able to calculate reasonable chemical formulas for smectite, chlorite, or chlorite/smectite minerals using the microprobe wt% oxide data. This may reflect disorder within the phyllosilicate structures or the presence of additional poorly ordered mineral phases associated with the phyllosilicates, such as Fe and Al oxyhydroxides, that were not recognized by X-ray diffraction analysis.

The kaolinite-free smectite samples in the <2 μm fraction (B, C, and Cgv; Table 1) are enriched in all cations except aluminum relative to the kaolinite-bearing smectite samples. This is not surprising, as kaolinite has only very minor substitution for Al within the octahedral sheet (Moore and Reynolds, 1997). Based on the chemical compositions of the relatively pure phyllosilicates in the <2 μm fraction, chemical formulas for samples from layers B, Cgv, and C are presented in Table 1. These chemical formulas correspond to montmorillonite. Chemical formulas for samples from layers D and E were not calculated due to the presence of kaolinite in these samples.

The <2 μm fraction has a higher wt% $H_2O$ than the corresponding whole-rock fraction for each horizon (Table 1). All of the <2 μm samples have similar wt% $H_2O$ that correspond to expected $H_2O$ yields for iron-rich montmorillonite (~4.90 wt%), with the exception of a sample from the unweathered basalt (A: 1.18 wt%) and the outer rind of the spheroidally weathered zone (D: 5.41 wt%).

The chemical composition of the goethite-rich sample Tri3g is presented in Table 3. $Fe_2O_3$

TABLE 2. WT% OXIDES OF PHYLLOSILICATES IN PARENT BASALT DETERMINED BY ELECTRON MICROPROBE

| Sample | $Na_2O$ | MgO | $Al_2O_3$ | $SiO_2$ | $K_2O$ | CaO | $TiO_2$ | $MnO_2$ | FeO | Total |
|---|---|---|---|---|---|---|---|---|---|---|
| 264b1 | 0.47 | 14.13 | 13.50 | 32.24 | 0.18 | 0.55 | 0.00 | 0.17 | 25.66 | 86.89 |
| 264b1a | 0.56 | 14.15 | 14.17 | 33.90 | 0.23 | 0.51 | 0.03 | 0.13 | 24.47 | 88.15 |
| 264b1b | 0.35 | 13.37 | 12.32 | 31.46 | 0.15 | 0.77 | 0.01 | 0.09 | 26.05 | 84.58 |
| 264b1c | 0.38 | 13.60 | 12.81 | 33.05 | 0.16 | 0.49 | 0.05 | 0.12 | 25.90 | 86.57 |
| 264b2a | 0.14 | 14.25 | 13.30 | 33.35 | 0.30 | 0.78 | 0.00 | 0.09 | 26.07 | 88.27 |
| 264b2b | 0.19 | 14.67 | 13.96 | 32.54 | 0.33 | 0.64 | 0.06 | 0.20 | 25.07 | 87.66 |
| 264b2c | 0.19 | 13.93 | 12.83 | 32.10 | 0.29 | 0.81 | 0.03 | 0.13 | 26.87 | 87.18 |
| 264b3a | 0.16 | 5.28 | 8.67 | 14.31 | 0.07 | 0.83 | 2.12 | 0.39 | 47.66 | 79.49 |
| 264b4a | 2.14 | 0.39 | 8.22 | 18.98 | 2.10 | 2.60 | 13.97 | 2.92 | 42.21 | 93.53 |
| 264b5a | 0.47 | 15.41 | 15.43 | 35.10 | 0.40 | 0.40 | 0.10 | 0.17 | 22.41 | 89.89 |
| 264b5b | 0.37 | 14.11 | 15.25 | 34.59 | 0.52 | 0.38 | 0.11 | 0.21 | 21.67 | 87.21 |
| 264b5c | 0.28 | 13.77 | 11.87 | 27.89 | 0.26 | 0.30 | 0.11 | 0.26 | 22.28 | 77.02 |
| 264b5d | 0.35 | 15.67 | 15.34 | 34.06 | 0.25 | 0.49 | 0.10 | 0.08 | 21.74 | 88.08 |
| 20241a | 0.16 | 5.37 | 13.56 | 56.57 | 4.44 | 0.54 | 0.00 | 0.00 | 12.78 | 93.43 |
| 264a1 | 6.50 | 0.70 | 11.52 | 38.11 | 1.94 | 14.34 | 5.07 | 1.33 | 10.51 | 90.01 |
| 264a2 | 4.69 | 1.07 | 13.43 | 43.93 | 3.54 | 10.54 | 1.92 | 0.52 | 5.73 | 85.37 |
| 264a3 | 0.22 | 13.41 | 14.02 | 28.75 | 0.17 | 0.60 | 0.48 | 0.28 | 30.05 | 87.98 |
| 264a4 | 0.37 | 13.25 | 13.94 | 27.80 | 0.18 | 0.57 | 0.40 | 0.31 | 28.61 | 85.42 |
| 264a5_1 | 0.31 | 13.70 | 13.43 | 31.75 | 0.16 | 0.59 | 0.00 | 0.14 | 26.64 | 86.72 |
| 264a5_2 | 0.48 | 12.33 | 13.43 | 33.26 | 0.38 | 0.40 | 0.00 | 0.18 | 25.73 | 86.19 |
| 264a5_3 | 0.27 | 14.66 | 12.54 | 32.13 | 0.10 | 0.38 | 0.08 | 0.13 | 27.39 | 87.69 |
| 264a5_4 | 0.38 | 14.40 | 12.82 | 32.21 | 0.17 | 0.38 | 0.03 | 0.13 | 27.46 | 87.98 |
| 264a5_5 | 0.45 | 14.28 | 13.24 | 32.82 | 0.17 | 0.50 | 0.08 | 0.13 | 26.53 | 88.21 |

TABLE 3. WT% OXIDES, MOLE FRACTION OF OXYGEN FROM GOETHITE IN Tri3g

| Analysis | Bulk Fe oxide | Residue | Goethite end member |
|---|---|---|---|
| $\delta^{18}O_{SMOW}$ | 2.7‰ | 9.0‰ | 2.3‰ |
| $\delta D_{SMOW}$ | –126‰ | –84‰ | –132‰ |
| $X(O)_{Fe}$ | 0.990 | | |
| $Na_2O$ | B.D. | | |
| MgO | B.D. | | |
| $Al_2O_3$ | 1.37 | | |
| $SiO_2$ | 1.92 | | |
| $P_2O_5$ | 1.82 | | |
| $K_2O$ | 0.34 | | |
| CaO | 0.10 | | |
| $TiO_2$ | 0.08 | | |
| $Fe_2O_3$ | 93.85 | | |
| wt% $H_2O$ | 7.10 | 2.11 | |

*Note*: As determined from ICP-OES analyses, manometric determination of wt% $H_2O$ in Tri3g, and Citrate-Bicarbonate-Dithionite-treated residue, measured oxygen and hydrogen isotope compositions of Tri3g and CBD residue, and calculated end-member isotopic compositions for goethite in sample. B.D.—concentrations below detection limits.

is the dominant oxide phase with very minor concentrations of $SiO_2$ and $Al_2O_3$ in a ratio of ~2:1. This is consistent with X-ray diffraction analysis, in which goethite is the predominant crystalline phase with trace 2:1 phyllosilicates.

## Isotopic Composition

The $\delta^{18}O$ values of calcite amygdules from the Triassic weathering profile are presented in Table 4 and Figure 4C. Calcite $\delta^{18}O_{SMOW}$ values are consistent throughout the profile, varying between 16.0‰ and 12.7‰.

The $\delta^{18}O$ and $\delta D$ values for the bulk and residue fractions of the goethite-rich samples are presented in Table 3. The residue remaining after goethite dissolution has more positive $\delta^{18}O$ and $\delta D$ values than the bulk fraction. The mole fraction of oxygen values in this sample was used to calculate the end-member goethite $\delta^{18}O$ values by mass balance (Yapp, 1998), in which:

$$\delta^{18}O_{bulk} = X(O)_{Fe} * \delta^{18}O_{Fe} + X(O)_{residue} * \delta^{18}O_{residue}$$

and

$$1 = X(O)_{Fe} + X(O)_{residue}.$$

It was assumed that all of the analyzed iron in the sample was goethite. If there is some amount of Fe in the octahedral layer of the trace 2:1 phyllosilicate or minor amounts of hematite associated with the goethite, it would introduce some error in the calculated $X(O)_{Fe}$ value. However, there is no evidence for hematite in the X-ray diffraction data. Furthermore, if the composition of the phyllosilicate associated with the Fe oxide sample is chemically similar to phyllosilicate in the overlying soil horizon, the maximum uncertainty of $X(O)_{Fe}$ attributed to goethite is less than one-half of one percent of the reported value in Table 3. The hydrogen isotopic composition of end-member goethite in Tri3g was determined by a mass balance calculation similar to that of the oxygen calculations, which considers the difference in the measured wt% $H_2O$, $\delta D$ values of the bulk and residue samples, and the calculated mole fraction of hydrogen, $X(H)_{Fe}$, in goethite. The end-member $\delta^{18}O$ and $\delta D$ values of Tri3g goethite are reported in Table 3 and Figure 4C.

The $\delta^{18}O$ and $\delta D$ values of phyllosilicates in the <2 μm fraction of the weathering profile and the bulk fraction of the underlying basalt are presented in Table 4 and Figure 4C. The oxygen isotopic composition of the <2 μm fraction ranges from 14.6‰ to 15.6‰ (mean value of 15.1 ± 0.5‰), which is considerably enriched over the parent basalt ($\delta^{18}O$ = 8.2‰). The hydrogen isotope composition of the phyllosilicates in the <2 μm fraction exhibit similar values throughout the profile, with a mean value of –74 ± 3‰. However, $\delta D$ values in this fraction show a small isotopic enrichment with increased weathering as indicated by more negative values (–81‰) in the parent basalt (A) compared to the clay-rich layers of the profile (–71‰ to –78‰; Table 4).

## DISCUSSION

Spheroidal features, amygdaloidal calcites, and smectites are commonly associated with near-surface and relatively low-temperature

TABLE 4. $\delta^{18}O$ AND $\delta D$ VALUES OF BULK BASALT, PHYLLOSILICATES (<2 μm FRACTION AND AMYGDULES), AND CALCITES

| Sample | Mineralogy | $\delta D_{SMOW}$ | $\delta^{18}O_{SMOW}$ |
|---|---|---|---|
| A | Bulk basalt | –81‰ | 8.2‰ |
| B | <2 μm montmorillonite | –71‰ | 15.4‰ |
| B | Calcite (n = 1) | - | 16.0‰ |
| C | <2 μm montmorillonite | –77‰ | 15.6‰ |
| C | Calcite (n = 2) | - | 12.7 ± 0.1‰ |
| Cgv | montmorillonite | –72‰ | 14.5‰ |
| D | <2 μm montmorillonite | –78‰ | 14.6‰ |
| D | Calcite (n = 1) | - | 13.7‰ |
| E | <2 μm montmorillonite | –72‰ | 15.6‰ |

hydrothermal (e.g., Yiu and Chang, 1999) and/or meteoric weathering environments ("onion-skin weathering"; Retallack, 1990). However, the morphology, mineralogy, and chemical compositions of the uppermost weathered zone (layer E; Css horizon) that developed on the Triassic-age basalt are indicative of pedogenesis. Wedge-shaped aggregate structure and slickensides in the Css horizon are characteristic of subsurface horizons that form under seasonal soil moisture regimes (Buol et al., 1997; Soil Survey Staff, 1998). The occurrence of these features within a montmorillonite-rich matrix suggests it formed as a Vertisol (Soil Survey Staff, 1998). Vertisols typically form on flat terrain with strongly contrasted wet and dry seasonal or monsoon-type climates (Singer et al., 1994; Buol et al., 1997). Repeated wetting and drying of expandable 2:1 phyllosilicate minerals leads to shearing of plastic soil materials and slickenside formation. Vertisols require a period of soil moisture deficit and sparse vegetation in order to maintain a high concentration of basic cations, thereby preserving expandable clay minerals in the soil matrix (Duchaufour, 1982; Retallack, 1990).

The chemical composition of the weathered zone indicates a significant loss of base cations, suggesting at least a moderate degree of alteration. This degree of pedogenic weathering requires leaching of minerals within the soil, facilitated through percolating meteoric waters, similar to bisiallitization-type weathering that is predominant in winter-wet and summer-dry soils forming in Mediterranean climates (Tardy, 1971). Moreover, the clay mineral composition of the paleosol profile, in which smectite with a chemical composition similar to montmorillonite dominates, is similar to that of modern soils that form in semihumid Mediterranean climates. Trace amounts of 1:1 phyllosilicate in the outer rind of the Cr horizon (D) and the Css horizon (E) suggest soil leaching and alteration of preexisting smectite to more stable, base-depleted kaolinite. This style of mineralogical and chemical alteration is found in Vertisols that form on stable, well-drained landscapes with relatively high rainfall (>600 mm/yr; Singer and Ben-Dor, 1987) and suggests similar conditions may have been present while the Late Triassic basalt flow underwent surficial weathering and pedogenesis.

As mentioned, carbonate is present in the parent basalt and spheroidal weathering layer, but absent in the overlying Css horizon. Furthermore, there is some petrographic evidence to indicate that carbonate became undersaturated and dissolved in portions of the profile. This strongly suggests that carbonate was leached from the Css horizon as a result of increased weathering in this portion of the profile with respect to the underlying spheroidal zone and parent basalt. A study by Royer (1999) demonstrated that soil carbonate will not accumulate if precipitation exceeds 760 mm/yr. This value is in reasonable accord with the necessary amount of precipitation required for formation of kaolinite in these types of soils (Singer and Ben-Dor, 1987). Furthermore, using the geochemical climofunction of soil alumina, soda, lime, and magnesia (Sheldon et al., 2002) in the bulk fraction of the weathered layers (Table 1) results in a calculated range of precipitation between 710 and 1080 mm/yr. By analogy with these modern data sets, rainfall was sufficiently high to leach carbonate from the paleosol profile during latter stages of weathering.

Although basaltic parent material is devoid of quartz, many soils developing on basalt contain this mineral as a result of eolian deposition of fine silt-sized grains during dry and windy episodes (Singer, 1978; Singer et al., 1994). Thus, the presence of quartz in the most highly weathered layers (D and E) of the Triassic paleosol is interpreted to indicate an eolian sediment input. In spite of the fact that precipitation was high enough to actively leach carbonate from the soil profile, the presence of eolian quartz suggests that conditions were intermittently dry.

The goethite-rich Fe oxide sample taken from below the spheroidal weathering zone (Cr) has 0% $Al^{3+}$ substitution within the goethite lattice. This is not consistent with a soil-forming environment, in which $Al^{3+}$ substitution is invariably higher (5–30 mol%) than that observed in this sample (Siehl and Thein, 1989). Rather, the lack of $Al^{3+}$ in goethite suggests groundwater deposits or orstein. This goethite likely formed in the water-saturated portion of the soil or during subsequent burial. This proposed timing of goethite formation is corroborated by micromorphologic textures deduced from petrographic analysis that indicate goethite formed concomitant with phyllosilicate formation (Fig. 5C) or soon after, occurring as a nearly monomineralic phase that replaced primary igneous oxides (Fig. 5D) or replaced preexisting calcite amygdules.

## Isotopic Inferences

Lawrence and Taylor (1972) found that, in general, the $\delta^{18}O$ values of the weathering products at or near Earth's surface are significantly higher than those of volcanic parent materials due to chemical reaction with meteoric waters at relatively low temperatures. In addition, it was observed that the $\delta D$ values of the weathering products may be drastically different from those found in the parent material. We observe a similar oxygen isotope enrichment of the montmorillonites relative to the parent basalt (Fig. 4C). Although paleosol phyllosilicate $\delta D$ values are more positive than the parent basalt, the difference is relatively small (Table 4; Fig. 4C). The $\delta D$ value of the bulk basalt likely results from secondary phyllosilicates (Fig. 6) with similar $\delta D$ values to montmorillonites in the weathered layer.

The oxygen and hydrogen isotope fractionation factors estimated for smectite likely provide a reasonable representation for the phyllosilicates analyzed in this study, even though some samples also contain kaolinite (E and D). The chemical composition of the <2 μm fraction confirms that the contribution of oxygen or hydrogen from kaolinite to the bulk phyllosilicate fraction in samples D and E is very small (<5 wt%) and will not result in a measured isotope value analytically discernable from the end-member smectite value (e.g., Savin and Lee, 1988). Therefore, smectite-water fractionations are used for paleotemperature estimates using the measured isotopic composition of the pedogenic phyllosilicates.

The $\delta^{18}O$ and $\delta D$ values of meteoric precipitation are controlled by several climatic parameters, especially temperature, "rain-out effect," and the rain-out history of the air mass (Dansgaard, 1964). Surficial weathering occurs as precipitation interacts with rock surfaces and infiltrates into the shallow subsurface. Numerous studies have documented that pedogenically derived minerals form in isotopic equilibrium with soil water, which in turn is closely related to the isotopic composition of meteoric precipitation (Lawrence and Taylor, 1971, 1972; Cerling and Quade, 1993; Yapp, 1993a). Thus, it is expected (and has been demonstrated; Yapp, 2000) that the $\delta D$ and $\delta^{18}O$ values of minerals formed at Earth's surface will define an array roughly parallel to the meteoric water line. By inference, $\delta D$ and $\delta^{18}O$ values of the Triassic minerals may be an important source of paleoclimate information. Furthermore, if the various alteration products within this paleosol profile formed in isotopic equilibrium, then the oxygen isotopic composition of these minerals may be used to calculate the temperature at which the minerals formed.

In this study, there are five different isotopic fractionation equations that apply to calculation of ancient water $\delta D$ and $\delta^{18}O$ values and temperatures of mineralization (T in degrees Kelvin):

Smectite-water oxygen ($^{18}\alpha$) and hydrogen ($^{D}\alpha$) isotope fractionation equations:

$$10^3 \ln(^{18}\alpha) = (2.60 \times 10^6/T^2) - 4.28 \quad \text{(Savin and Lee, 1988).} \quad (1)$$

$$10^3 \ln(^{D}\alpha) = (-7.50 \times 10^6/T^2) + 27.37 \quad \text{(Capuano, 1992).} \quad (2)$$

Goethite-water oxygen and hydrogen isotope fractionation equations:

$$10^3 \ln(^{18}\alpha) = (1.63 \times 10^6/T^2) - 12.3 \quad \text{(Yapp, 1990).} \quad (3)$$

$$^{D}\alpha = 0.905 \text{ (Yapp, 1987).} \quad (4)$$

Calcite-water oxygen isotope fractionation equation:

$$10^3 \ln(^{18}\alpha) = (2.78 \times 10^6/T^2) - 2.89 \quad \text{(O'Neil et al., 1969).} \quad (5)$$

Combination of the oxygen isotope fractionation equations for smectite, goethite, and calcite indicate that none of these minerals formed in isotopic equilibrium. This is surprising, as other work on modern soil-weathering systems (Girard et al., 2000; Yapp, 1997) and paleosols (Yapp, 1993b) suggests that isotopic equilibrium, or near-equilibrium values, should be approached by different minerals in a soil system. Isotopic data from these Triassic minerals therefore suggest formation (1) at different temperatures, (2) from waters with different isotopic composition, (3) with subsequent postpedogenic alteration, or (4) a combination of these effects.

Yapp (1987, 1993a, 2000) and Delgado and Reyes (1996) proposed that the δD and $\delta^{18}O$ values of ancient goethites and smectites, respectively, might serve as single-mineral paleothermometers. For this calculation, it is assumed that these minerals formed in isotopic equilibrium with meteoric waters and that the isotopic composition of the samples has not changed since their formation.

The empirical relationship between hydrogen and oxygen isotopes in meteoric waters is well known. The mathematical expression for this relationship is approximated by:

$$\delta D_w = 8 \times \delta^{18}O_w + 10, \quad (6)$$

where the subscript "w" represents meteoric water. As indicated by equation 4, goethite-water hydrogen isotope fractionation is not sensitive to temperature differences in the range 25 to 148 °C, whereas goethite-water oxygen isotope fractionation (equation 3) is temperature dependent. Thus, measured δD and $\delta^{18}O$ values of a goethite may be used in combination with equations 3, 4, and 6 to calculate the temperature of goethite crystallization:

$$T = \left( \frac{1.63 \times 10^6}{\Delta^{18}O_{g-w} + 12.3} \right)^{\frac{1}{2}}$$

$$10^3 \ln^{18}\alpha \approx \delta^{18}O_g - \delta^{18}O_w = \Delta^{18}O_{g-w};$$

$$\delta^{18}O_w = \left[ \frac{\frac{(1000 + \delta D_g)}{^{D}\alpha} - 1000}{8} \right], \quad (7)$$

where $\delta D_g$ and $\delta^{18}O_g$ are the measured hydrogen and oxygen isotope composition, respectively, of goethite and $^{D}\alpha$ is the stable hydrogen isotope fractionation factor between goethite and water (0.905). For the goethite sample analyzed in this study, the measured $\delta D_g$ and $\delta^{18}O_g$ are –132 ± 4‰ and 2.7 ± 0.2‰, respectively. These values correspond to a goethite crystallization temperature of 6 ± 3 °C. The corresponding $\delta^{18}O$ and δD of meteoric water in equilibrium with this goethite were –6.4 ± 0.5‰ and –41 ± 4‰, respectively. Such a temperature and isotopic composition is consistent with a low-temperature, meteoric water–dominated soil-weathering system.

Using equations 1, 2, and 6, Delgado and Reyes (1996) proposed the following equation as a single-mineral geothermometer for smectites:

$$3.54 \times 10^6/T^2 = \delta^{18}O_{sm} - 0.125\delta D_{sm} + 8.95, \quad (8)$$

where $\delta^{18}O_{sm}$ and $\delta D_{sm}$ are the measured smectite $\delta^{18}O$ and δD values. The range of δD and $\delta^{18}O$ values of the Triassic-age <2 µm fraction phyllosilicates are –78‰ to –71‰ and 14.5‰ to 15.6‰, respectively (Figs. 4B and 4C; Table 4), corresponding to a range of temperatures from 49 to 57 °C. These calculated temperatures are significantly higher than those calculated from the coexisting goethite and inconsistent with a pedogenic origin. However, the calculated water isotope δD and $\delta^{18}O$ values in equilibrium with these montmorillonites range from –29 ± 4‰ to –36 ± 4‰ and –4.8 ± 0.5‰ to –5.7 ± 0.5‰, respectively. Thus, the calculated δD and $\delta^{18}O$ of water in equilibrium with these phyllosilicates are, within analytical uncertainty, indistinguishable from the δD and $\delta^{18}O$ values of water in equilibrium with the coexisting goethite sample.

A similar alteration history of basalts has been observed in the Miocene–Early Pliocene Penghu basalts of Taiwan. Based on the δD and $\delta^{18}O$ values of montmorillonitic and saponitic amygdules and fissure-fills, Yiu and Chang (1999) concluded that these minerals precipitated from meteoric groundwater or mixed groundwater and seawater under late-stage hydrothermal temperatures ranging from 20 to 50 °C. The Late Triassic Ischigualasto Formation was deposited in a closed continental basin. Therefore, seawater probably did not impact groundwater isotopic compositions. The similar calculated temperatures from the Late Triassic smectites and the Penghu basalt alteration products suggest that these deposits share a similar late-stage hydrothermal origin in the presence of meteoric waters. Furthermore, unless the measured smectite and goethite δD and $\delta^{18}O$ compositions from the Late Triassic weathering profile are coincidental, such values are a strong indication that these minerals formed from the same *meteoric* waters with similar isotopic composition, but at different temperatures.

Although the Penghu basalts are deeply weathered, there is no significant soil development, kaolinite, or goethite associated with these deposits. However, the development of slickensides and wedge-shape aggregate structure in the Css horizon of the Triassic weathering profile is a clear indication that soil development did take place upon and within the hydrothermally altered, smectite-rich Ischigualasto basalt flow. Montmorillonite is a common soil mineral in subtropical and temperate climates (e.g., Moore and Reynolds, 1997). Therefore, smectites that initially form in a hydrothermal environment that are subsequently incorporated into soil may not necessarily undergo mineralogical or isotopic alteration because there is no chemical force to facilitate such a change. In this regard, we consider the Triassic montmorillonites and their δD and $\delta^{18}O$ values to be inherited from preexisting low-temperature hydrothermal conditions, whereas trace amounts of kaolinite found in the most weathered layers (D and E) and dissolution of carbonate may represent incipient pedogenic weathering of a hydrothermal assemblage. Furthermore, the addition of goethite to the weathering profile likely occurred subsequent to hydrothermal activity, at relatively low temperatures, penecontemporaneous with pedogenesis. We interpret the paleotemperature of 6 ± 3 °C to be near a maximum estimate of mean annual surface-air temperature during Late Triassic soil formation. This reflects that shallow subsurface temperatures are typically ~1–2 °C warmer than mean annual surface temperatures (Buol et al., 1997), and that the isotopic composition of ancient goethites has been shown to retain primary values (Yapp, 1987, 1993a, 2000).

Calcites are not amenable to single-mineral paleothermometer calculations. However, if these calcites formed from the same meteoric water $\delta^{18}O$ values (–4.8‰ to –5.7‰) associated with coexisting smectite and goethite, then the isotopic compositions of the calcites may be used to directly calculate the temperature of calcite crystallization using equation 5. The $\delta^{18}O$ values of calcite amygdules from the Late Triassic weathering profile range from 12.7‰ to 16.0‰. These

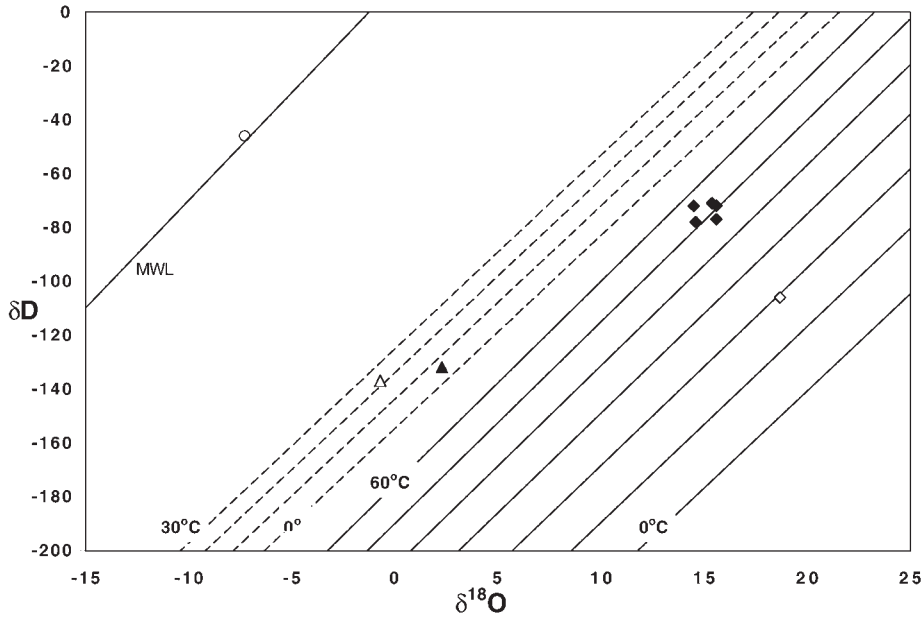


**Figure 9. δD vs. $\delta^{18}O$ plot of the measured isotopic composition of phyllosilicates and goethite from the Triassic weathering profile. Also shown are the meteoric waterline (MWL) and the calculated δD and $\delta^{18}O$ isotherms of smectite (solid lines) and goethite (dashed lines) in equilibrium with meteoric waters at 10 °C increments using the thermodynamic fractionation factors in equations 1–4. The Triassic phyllosilicates (filled diamonds) plot well above temperatures calculated for low-temperature, earth-surface conditions, whereas the goethite (solid triangle) plots at low temperatures consistent with a pedogenic origin. The open circle represents δD and $\delta^{18}O$ values of present-day springwater collected near the study area. The open diamond and triangle represent the calculated δD and $\delta^{18}O$ values of a montmorillonite and goethite, respectively, in isotopic equilibrium with the springwater. See text.**

calcite $\delta^{18}O$ values correspond to an approximate range of temperatures between 60 and 100 °C for calcite formation. This range of temperatures is in reasonable accord with temperatures of calcite crystallization observed in other hydrothermal systems (e.g., Clayton and Epstein, 1961).

The calculated temperatures of calcite, smectite, and goethite crystallization in the Late Triassic weathering profile correspond well with the inferred paragenetic sequence of mineral formation determined petrographically (Figs. 5A–D). In this sequence, calcite is the first mineral to form after basalt emplacement and therefore likely formed at the highest temperatures (~60–100 °C), smectite precipitation followed at lower hydrothermal temperatures (49 to 57 °C), and finally goethite precipitation at ambient Earth surface temperature (6 ± 3 °C).

### *Retention of Primary δD Compositions?*

Numerous studies have focused on the exchangeability of oxygen and hydrogen isotopes in phyllosilicate minerals (O'Neil and Kharaka, 1976; Bird and Chivas, 1988; Kyser and Kerrich, 1991; Mizota and Longstaffe, 1996). Results from both laboratory and field studies indicate that mineral hydrogen may be susceptible to postformational isotopic exchange, through the process of proton exchange, in the absence of a mineralogic or chemical change. However, Sheppard and Gilg (1996) noted serious problems with empirical evidence for low-temperature hydrogen exchange. Subsequently, Gilg (2000) made a compelling argument for the retention of original δD in Triassic through Tertiary kaolinites from southern Germany. Despite this, theoretical considerations and experimental data indicate that a <2 μm clay mineral can completely reequilibrate hydrogen isotopes at 25 °C after only a few million years (Kyser and Kerrich, 1991). Thus, the measured δD values of the Triassic phyllosilicates may reflect those of postdepositional fluids to which they were exposed.

There are no historical isotope records of meteoric rainfall near the study area. However, the measured δD and $\delta^{18}O$ values of water from a spring (20 °C) near Ischigualasto Provincial Park are –46‰ and –7.3‰, respectively. These values lie upon the meteoric waterline and are likely very near the values for the weighted mean isotopic composition of meteoric rainfall and soil temperature in this area (e.g., Clark and Fritz, 1997). The corresponding δD and $\delta^{18}O$ values for a hypothetical smectite in isotopic equilibrium with the springwaters at 20 °C are –102‰ and 18.8‰, whereas the δD and $\delta^{18}O$ values for a hypothetical goethite are –137‰ and –0.7‰ (Fig. 9). Therefore, the measured hydrogen isotope values of the montmorillonites are 24‰–31‰ more positive, and the goethite 5‰ more positive, than the expected value for complete proton exchange with local meteoric waters. Gilg (2000) noted that it is very difficult, probably even impossible, to prove whether there has been any hydrogen isotopic exchange in phyllosilicates with younger waters. Nonetheless, that these two minerals are isotopically heavier than anticipated values for proton exchange with ambient modern meteoric waters suggests they preserve a record of preexisting, ancient conditions. Furthermore, we consider the fact that the montmorillonites and coexisting goethite apparently formed from the same meteoric waters, compelling evidence that these minerals retain Triassic hydrogen isotope compositions.

### *Paleoclimate Interpretation*

Figure 10 presents the measured $\delta^{18}O$ compositions of meteoric waters versus mean annual surface temperature for each site in the International Atomic Energy Association (IAEA) global database (Rozanski et al., 1993). As mentioned, the maximum range of meteoric water $\delta^{18}O$ values in equilibrium with the Triassic minerals is –6.9‰ to –4.3‰. Furthermore, surface temperatures ranged from 6 ± 3 °C. Only two sites in the modern global database lie within this range of temperatures and $\delta^{18}O$ values. These sites are Marion Island (South Pacific; ~47° S) and Lista (Norway; ~58° N). It is interesting to note that the latitudes of these modern sites are similar to the paleolatitude of the Late Triassic Ischigualasto basin (40°–50° S; Scotese and Golonka, 1992; Smith et al., 1994). These sites may serve as modern analogs for the Late Triassic climate system associated with this weathering profile. Both sites have relatively high mean annual precipitation, Marion Island with 2452 mm/yr and Lista with 1025 mm/yr. Furthermore, both of these sites occur in coastal regions, proximal to a marine-derived source of precipitation.

As noted earlier, the chemical composition of the alteration products in this weathering profile corresponds to bisiallitization weathering in modern soils (Tardy, 1971) with a calculated precipitation range between 710 and 1080 mm/yr (cf. Sheldon et al., 2002). However, if this deposit represents incipient pedogenic overprinting of a hydrothermal deposit, the

elemental composition of weathering products may not represent a low-temperature soil-forming environment. Rather, the elemental and mineralogical composition of this deposit may be more representative of a relict hydrothermal system that never reached chemical equilibrium with the soil-forming environment. Therefore, soil geochemical climofunctions may result in erroneous paleoclimate reconstructions for this weathering system.

Pedogenically derived kaolinite and dissolution of carbonate from the Triassic paleosol profile suggest precipitation exceeded 760 mm/yr. This conforms to precipitation values inferred from modern sites with similar surface air temperatures and isotopic ranges of meteoric waters calculated from the Triassic minerals. However, the smectite and goethite isotopic data in this weathering profile suggest that precipitation may have been >1000 mm/yr, higher than values inferred by carbonate dissolution (Royer, 1999) and geochemical transfer functions (Sheldon et al., 2002). Stable isotope evidence, in conjunction with a Vertisol paleosol morphology, suggests a quite humid and cool climate characterized by seasonal precipitation during deposition of the Late Triassic, lower Ischigualasto Formation.

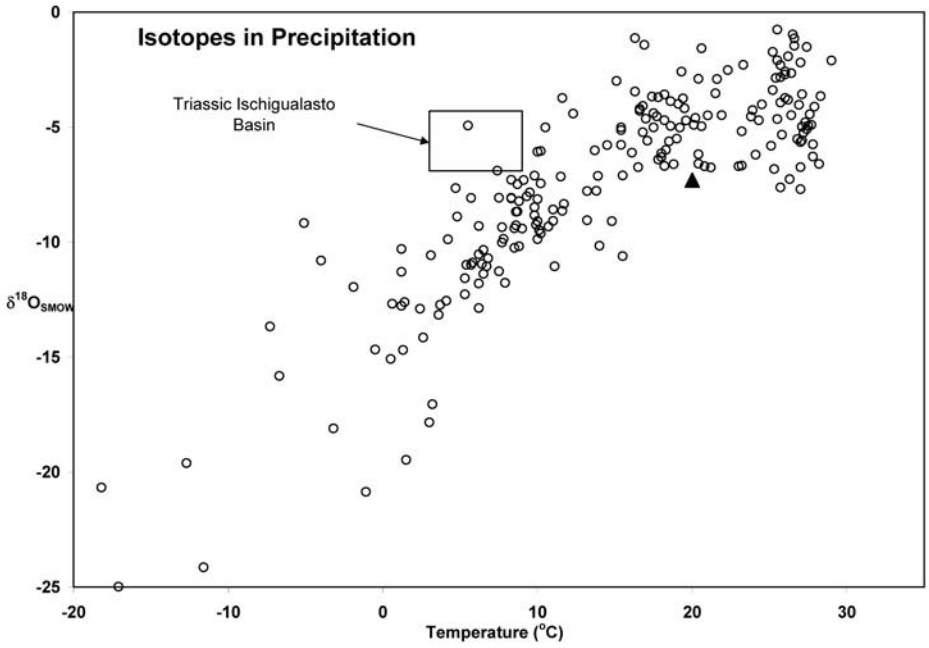


**Figure 10. Plot of the $\delta^{18}O$ values of meteoric precipitation vs. temperature (open circles) for each of the sites in the International Atomic Energy Association (IAEA) global database (Rozanski et al., 1993). The solid triangle represents the oxygen isotopic composition and temperature of spring water within the vicinity of the study area. The open box represents the maximum range of $\delta^{18}O$ compositions of paleo-soil water estimated from the measured $\delta^{18}O$ values of phyllosilicates and goethite and estimated paleotemperature based on goethite $\delta D$ and $\delta^{18}O$. See text.**

## CONCLUSIONS

Integrated field, mineral, chemical, and stable isotope analysis of a weathered horizon developed on Carnian-age basalt in the Ischigualasto basin, northwest Argentina, indicates a pedogenic origin. The presence of wedge-shaped aggregate structure and slickensides indicate it was a Vertisol that formed on a well-drained landscape with seasonal soil moisture conditions. Loss of carbonate and incipient development of kaolinite in the soil profile suggest precipitation may have been in excess of 760 mm/yr. Quartz in the paleosol profile may record episodes of eolian deposition in the basin.

Chemical trends within the paleosol profile are consistent with those observed in modern weathering profiles from seasonal, subhumid climates. Despite this, none of the authigenic minerals from the weathering profile exhibits isotopic equilibrium, which is not consistent with a pedogenic origin. However, on the basis of the combined $\delta D$ and $\delta^{18}O$ values, these minerals apparently formed from meteoric waters of a similar isotopic composition (maximum range: $\delta D = -24‰$ to $-45‰$; $\delta^{18}O = -4.3‰$ to $-6.9‰$), but at very different temperatures. Calcite and montmorillonite may have formed over a range of temperatures from 60 to 100 °C and 49 to 57 °C, respectively, during waning stages of hydrothermal alteration, whereas goethite formed at 6 ± 3 °C during supergene, or pedogenic, weathering. Modern regions with similar isotope compositions of meteoric water and earth-surface temperatures are characterized by rainfall in excess of 1000 mm/yr and may indicate similar conditions for the Late Triassic Ischigualasto–Villa Unión basin.

The paragenetic sequence of hydrothermal to supergene weathering in this basalt flow is complex and may be representative of a general phenomenon in continental rift basalts. Despite these complications, this study shows great potential for these geologically abundant lithologies as records of paleoclimate.

### ACKNOWLEDGMENTS

We are indebted to Oscar Alcober from the San Juan National University, San Juan, Argentina, for providing us with access to and expertise in the field area. We also thank Kelley Moore and Todd Shipman for assistance in the field. Lynn Soreghan, Brian Stewart, Michael Engle, Crayton Yapp, and one anonymous reviewer provided input that considerably improved the quality of this manuscript. This project was partially funded by Grants-in-Aid to N. Tabor from the Geological Society of America (GSA), American Association of Petroleum Geologists (AAPG), Society for Sedimentary Geology (SEPM), and Sigma Xi, as well as a National Science Foundation (NSF) grant EAR-9814640 to I.P. Montañez, and a National Geographic grant to Judy Parrish.

### REFERENCES CITED

Alcober, O., 1996, Revision de los crurotarsi, estratigrafia y tafonomia de la Formacion Ischigualasto [Ph.D. thesis]: San Juan, Argentina, Universidad Nacional de San Juan, 260 p.

Bird, M.I., and Chivas, A.R., 1988, Stable isotope evidence for low-temperature weathering and post-formational hydrogen-isotope exchange in Permian kaolinites: Chemical Geology, v. 72, p. 249–265.

Brindley, G.W., 1980, Order-disorder in clay mineral structures, *in* Brindley, G.W., and Brown, G., eds., Crystal structures of clay minerals and their X-ray identification: Mineralogical Society [London] Monograph 5, p. 95–125.

Buol, S.W., Hole, F.D., McCracken, R.J., and Southard, R.J., 1997, Soil genesis and classification: Ames, Iowa State University Press, 527 p.

Capuano, R.M., 1992, The temperature dependence of hydrogen isotope fractionation beween clay minerals and water: Evidence from a geopressured system: Geochimica et Cosmochimica Acta, v. 56, p. 2547–2554.

Cerling, T.E., and Quade, J., 1993, Stable carbon and oxygen isotopes in soil carbonates, *in* Swart, P.K., et al., eds., Climate change in continental isotopic records: Washington, D.C., American Geophysical Union Monograph 78, p. 217–231.

Clark, I.D., and Fritz, P., 1997, Environmental isotopes in hydrogeology: New York, Lewis Publishers, 328 p.

Clayton, R.N., and Epstein, S., 1961, The use of oxygen isotopes in high-temperature geological thermometry: Journal of Geology, v. 69, p. 447–452.

Currie, B., Tabor, N., Shippman, T., Montanez, I.P., and Moore, K., 2001, Stratigraphic architecture of the Upper Triassic Ischigualasto Formation, Ischigualasto Provincial Park, northwestern Argentina: Geological Society of America Abstracts with Programs, v. 33, p. A75.

Dansgaard, W., 1964, Stable isotope in precipitation: Tellus, v. 16, p. 436–468.

Delgado, A., and Reyes, E., 1996, Oxygen and hydrogen isotope compositions in clay minerals; a potential

single-mineral paleothermometer: Geochimica et Cosmochimica Acta, v. 60, p. 4285–4289.

Duchaufour, P., 1982, Pedology, pedogenesis and classification: London, George, Allen, and Unwin, 448 p.

Gilg, H.A., 2000, D-H evidence for the timing of kaolinitization in NE Bavaria, Germany: Chemical Geology, v. 170, p. 5–18.

Girard, J.P., Feyssinet, P., and Chazot, G., 2000, Unraveling climatic changes from introprofile variation in oxygen and hydrogen isotopic composition of goethite and kaolinite in laterites: An integrated study from Yaou, French Guiana: Geochimica et Cosmochimica Acta, v. 64, p. 409–426.

Kyser, T.K., and Kerrich, R., 1991, Retrograde exchange of hydrogen isotopes between hydrous minerals and water at low temperatures, *in* Taylor, H.P., et al., eds., Stable isotope geochemistry: A tribute to Samuel Epstein: San Antonio, Texas, Geochemical Society Special Publication 3, p. 409–421.

Lawrence, J.R., and Taylor, H.P., Jr., 1971, Deuterium and oxygen-18 correlation: Clay minerals and hydroxides in Quaternary soil compared to meteoric water: Geochimica et Cosmochimica Acta, v. 35, p. 993–1003.

Lawrence, J.R., and Taylor, H.P., Jr., 1972, Hydrogen and oxygen isotope systematics in weathering profiles: Geochimica et Cosmochimica Acta, v. 36, p. 1377–1393.

Lopez, S.D., 1995, Estudio estratigraphico sequencial y oleogeoquimico del paleolago Ischichuca-Los Rastros [M.S. thesis]: San Juan, Argentina, Universidad Nacional de San Juan, 125 p.

Lopez-Gamundi, O.R., Alvarez, L., Andreis, R., Bossi, G.E., Espejo, I., Fernandez Seveso, F., Legarreta, L., Kokogian, K., Limarino, C.O., and Sessarego, H., 1989, Cuencas intermontanas: Cuencas Sedimentarias Argentinas, v. 189, p. 123–167.

Lopez-Gamundi, O.R., Espejo, I.S., Conaghan, P.J., Powell, C.McA., and Veevers, J.J., 1994, Southern South America, *in* Veevers, J.J., and Powell, C.McA., eds., Permian-Triassic Pangean basins and foldbelts along the Panthalassan margin of Gondwanaland: Boulder, Colorado, Geological Society of America Memoir 184, p. 281–329.

Milana, J.P., and Alcober, O., 1994, Modelo tectonosedimentario dee la cuenca triasica de Ischigualasto (San Juan, Argentina): Revista de la Asociacion Argentina, v. 49, p. 217–235.

Mizota, C., and Longstaffe, F.J., 1996, Origin of Cretaceous and Oligocene kaolinites from the Iwaizumi clay deposit, Iwate, northeastern Japan: Clays and Clay Minerals, v. 44, p. 408–416.

Monro, S.K., Loughnan, F.C., and Walker, M.C., 1983, The Ayrshire bauxitic clay: An allochthonous deposit?, *in* Wilson, R.C.L., ed., Residual deposits: Geological Society (London) Special Publication 11, p. 47–58.

Moore, D.M., and Reynolds, R.C., 1997, X-ray diffraction and the identification and analysis of clay minerals: New York, Oxford University Press, 378 p.

Moore, K.A., Tabor, N.J., Montanez, I.P., Currie, B.S., and Shipman, T., 2001, Paleoclimate reconstruction from the $\delta^{13}C$ carbonate proxies in Triassic paleosols and sediments, Ischigualasto Basin, Argentina: San Francisco, American Geophysical Union Abstracts with Programs, p. 237.

Odin, G.S., Battail, B., and Cingolani, C., 1982, NDS 187; Triassic; Carnian(?), K-Ar/whole-rock, Gondwana Province, *in* Odin, G.S., ed., Numerical dating in stratigraphy: Chichester, Wiley and Sons, p. 860.

O'Neil, J.R., and Kharaka, Y.K., 1976, Hydrogen and oxygen isotope exchange reactions between clay minerals and water: Geochimica et Cosmochimica Acta, v. 40, p. 241–246.

O'Neil, J.R., Clayton, R.N., and Mayeda, T.K., 1969, Oxygen isotope fractionation in divalent metal carbonates: Journal of Chemical Physics, v. 51, p. 5547–5558.

Ramos, V.A., and Kay, S.M., 1991, Triassic rifting and associated basalts in the Cuyo basin, central Argentina, *in* Harmon, R.S., ed., Andean magmatism and its tectonic setting: Boulder, Colorado, Geological Society of America Special Paper 265, p. 79–91.

Retallack, G.J., 1988, Field recognition of paleosols, *in* Reinhardt, J., and Sigleo, W.R., eds., Paleosols and weathering through geologic time: Principles and applications: Boulder, Colorado, Geological Society of America Special Paper 216, p. 1–20.

Retallack, G.J., 1990, Soils of the past: An introduction to paleopedology: Boston, Massachusetts, Unwin Hyman, 520 p.

Rodgers, R.R., Swisher, C.C., III, Sereno, P.C., Monetta, A.M., Forster, C.A., and Martinez, R.N., 1993, The Ischigualasto tetrapod assemblage (Late Triassic, Argentina), and $^{40}Ar/^{39}Ar$ dating of dinosaur origins: Science, v. 260, p. 794–797.

Royer, D.L., 1999, Depth to pedogenic carbonate horizon as a paleoprecipitation indicator?: Geology, v. 27, p. 1123–1126.

Rozanski, K., Araguas-Araguas, L., and Gonfiantini, R., 1993, Isotopic patterns in modern global precipitation, *in* Swart, P.K., et al., eds., Climate change in continental isotopic records: Washington, D.C., American Geophysical Union Monograph 78, p. 1–36.

Savin, S.M., and Epstein, S., 1970, The oxygen and hydrogen isotope geochemistry of clay minerals: Geochimica et Cosmochimica Acta, v. 34, p. 25–42.

Savin, S.M., and Lee, M., 1988, Isotopic studies of phyllosilicates, *in* Ribbe, P.H., Hydrous phyllosilicates: Reviews in Mineralogy, v. 19, p. 189–223.

Schulze, D.G., 1984, The influence of aluminum on iron oxides, VIII: Unit cell dimensions of Al-substituted goethites and estimation of aluminum from them: Clays and Clay Minerals, v. 32, p. 36–44.

Scotese, C.R., and Golonka, J., 1992, Paleogeographic atlas: Arlington, University of Texas, Paleomap Project, 20 p.

Sheldon, N.D., Retallack, G.J., and Tanaka, S., 2002, Geochemical climofunctions from North American soils and application to paleosols across the Eocene-Oligocene Boundary in Oregon: Journal of Geology, v. 110, p. 687–696.

Sheppard, S.M.F., and Gilf, H.A., 1996, Stable isotope geochemistry of clay minerals: Clay Minerals, v. 31, p. 1–24.

Siehl, A., and Thein, J., 1989, Minette-type ironstones, *in* Young, T.P., and Taylor, W.E., eds., Phanerozoic ironstones: Geological Society (London) Special Publication 46, p. 175–193.

Singer, A., 1978, The nature of basalt weathering in Israel: Soil Science, v. 125, p. 217–225.

Singer, A., and Ben-Dor, E., 1987, Origin of red clay layers interbedded with basalts of the Golan Heights: Geoderma, v. 39, p. 293–306.

Singer, A., Wieder, M., and Gvirtzman, G., 1994, Paleoclimate deduced from some early Jurassic basalt-derived paleosols from northern Israel: Palaeogeography, Palaeoclimatology, Palaeoecology, v. 111, p. 73–82.

Soil Survey Staff, 1998, Keys to Soil taxonomy: Washington, D.C., United States Department of Agriculture, Natural Resources Conservation Service, 326 p.

Stipanicic, P.N., and Bonaparte, J.F., 1979, Cuenca triasica de Ischigualasto-Villa Union (Provincias de La Rioga y San Juan), *in* Turner, J.C., ed., Segundo Simposio de Geologia Regional Argentina, 1: Cordoba, Academia Nacional de Ciencias, p. 523–575.

Tardy, Y., 1971, Characterization of the principal weathering types by the geochemistry of waters from some European and African massifs: Chemical Geology, v. 7, p. 253–271.

Uliana, M.A., and Biddle, K.T., 1988, Mesozoic-Cenozoic paleogeographic and geodynamic evolution of southern South America: Revista Brasileira de Geociencias, v. 18, p. 172–190.

Uliana, M.A., Biddle, K.T., and Cerdan, J., 1989, Mesozoic extension and the formation of Argentine sedimentary basins, *in* Balkwill, H.R., and Tankard, A.J., eds., Extensional tectonics and stratigraphy of the North Atlantic margins: Tulsa, Oklahoma, American Association of Petroleum Geologists Memoir 46, p. 599–614.

Valencio, D.A., Mendia, J.E., and Vilas, J.F., 1975, Palaeomagnetism and K-Ar ages of Triassic igneous rocks from the Ischigualasto-Ischichuca Basin and Puesto Viejo Formation, Argentina: Earth and Planetary Science Letters, v. 26, p. 319–330.

Yapp, C.J., 1987, Oxygen and hydrogen isotope variations among goethites (α-FeOOH) and the determination of paleotemperatures: Geochimica et Cosmochimica Acta, v. 51, p. 355–364.

Yapp, C.J., 1990, Oxygen isotopes in iron (III) oxides, 1, Mineral-water fractionation factors: Chemical Geology, v. 85, p. 329–335.

Yapp, C.J., 1993a, The stable isotope geochemistry of low temperature Fe (III) and Al "oxides" with implications for continental paleoclimates: Washington, D.C., American Geophysical Union Monograph 78, p. 285–294.

Yapp, C.J., 1993b, Paleoenvironment and the oxygen isotope geochemistry of ironstone of the upper Ordovician Neda Formation, Wisconsin, USA: Geochimica et Cosmochimica Acta, v. 57, p. 2319–2327.

Yapp, C.J., 1997, An assessment of isotopic equilibrium in geothites from a bog iron deposit and a lateritic regolith: Chemical Geology, v. 135, p. 159–171.

Yapp, C.J., 1998, Paleoenvironmental interpretations of oxygen isotope ratios in oolitic ironstones: Geochimica et Cosmochimica Acta, v. 62, p. 2409–2420.

Yapp, C.J., 2000, Climatic implications of surface domains in arrays of δD and $\delta^{18}O$ from hydroxyl minerals: Goethite as an example: Geochimica et Cosmochimica Acta, v. 64, p. 2009–2025.

Yiu, T.F., and Chang, S.S., 1999, Formation conditions of vesicle/fissure-filling smectites in Penghu basalts; a stable isotope assessment: Clay Minerals, v. 34, p. 381–393.

Manuscript Received by the Society 24 July 2002
Revised Manuscript Received 12 September 2003
Manuscript Accepted 28 September 2003

Printed in the USA